PCCP

ARTICLE TYPE

Cite this: DOI: 00.0000/xxxxxxxxxx

Adsorption of a single Pt atom on graphene: Spin crossing between physisorbed triplet and chemisorbed singlet states

Jeonghwan Ahn[a], Iuegyun Hong[a], Gwangyoung Lee[a], Hyeondeok Shin[b],Anouar Benali[b‡] and Yongkyung Kwon*[a]

Received Date
Accepted Date

DOI: 00.0000/xxxxxxxxxx

Diffusion Monte Carlo (DMC) calculations have been performed to study the adsorption of a single Pt atom on pristine graphene. We obtain the adsorption energy curves of a single Pt atom adsorbed at three different adsorption sites (bridge, on-top, hollow) as functions of the vertical distance from a graphene surface for both spin singlet and triplet states. The bridge-site adsorption in a singlet spin state is found to be energetically most stable, which is consistent with previous theoretical predictions. As the Pt atom moves away from a graphene surface, spin triplet states are favored over spin singlet states for all three adsorption sites, reflecting that the ground state of an isolated Pt atom is in a spin triplet state. Furthermore, our DMC calculations reveal local-minimum features in the triplet region which is understood to be due to van der Waals interaction between the Pt adatom and graphene. This provides a comprehensive understanding for a spin crossing from a physisorbed triplet state to a chemisorbed singlet state in the adsorption process of a single Pt atom on graphene.

1 Introduction

For the past decade, transition metal(TM)-graphene interfaces have been intensively studied for development of graphene-based nanoelectronics. Especially, nanostructures (or clusters) of TM atoms supported by graphene have drawn much attention because TM adatoms could provide various modes of functionalization to graphene through chemisorptions with a binding-energy scale of an order of eV. These systems were predicted to show some exotic phenomena such as a local doping and charge-impurity scattering[1,2], topological phases[3,4], and superconducting states[5], depending on the coverage of TM adatoms.

A graphene-supported Pt cluster has been proposed[6–13] as an alternative to the conventional Pt catalyst supported on carbonaceous materials such as activated carbon or carbon black[14]. The Pt-graphene system allows a controllable design of Pt nanostructure because of its well-defined crystalline structure, which could result in enhanced catalytic properties and better long-term stability against sintering than conventional Pt catalysts[15–17]. Furthermore, a series of preliminary experimental studies on the Pt-graphene systems elucidated their potential for electrocatalysts in direct methanol fuel cells[15,16] and proton-exchange membrane fuel cells for oxygen reduction[18] as well as hydrogen fuel cells[19]. A problem of using a Pt cluster in the catalytic reaction, however, is that its geometry prohibits a majority of Pt atoms in the core region from participating in the catalytic reaction with only the surface atoms involved in the reaction. In this regard, downsizing Pt clusters would be highly desirable to reduce an amount of Pt metal and to enhance the effective Pt utilization in the reaction process. For this purpose, single-atom catalysis of Pt supported by a graphene sheet has been pursued but its experimental realization has been extremely limited up to now[6].

Consequently, it is essential to understand the interaction between a single Pt atom and the graphene sheet. Most of theoretical studies for this system have been done with density functional theory (DFT) calculations[8–13] which lacked proper descriptions of electron-electron correlations, especially among localized Pt $5d$ electrons. Previous DFT studies reported that the interaction between Pt and graphene displayed a weak covalent character, accompanied by a little amount of charge transfer, about ~ 0.1 electron per Pt atom[9,11,13]. On the other hand, CCSD(T) and diffusion Monte Carlo (DMC) calculations[20] for a Pt-benzene half-sandwich complex, a fragment of a Pt-graphene system, showed the Pt binding curve featuring a single minimum in spin singlet state, along with a shoulder at longer adsorption distances that arises from spin crossing between the singlet and the triplet states. Since an analogous spin crossing is expected for the Pt-graphene system, one needs to consider both spin singlet and triplet states and to scan a wide range up to longer distances far away from the chemical bonding region for a complete un-

[a] Department of Physics, Konkuk University, Seoul 05029, Korea. Email: ykwon@konkuk.ac.kr
[b] Computational Science Division, Argonne National Laboratory, Argonne, Illinois 60439, USA Email: benali@anl.gov

derstanding of the adsorption process of a Pt atom on a graphene surface.

In order to understand the adsorption process of a Pt atom on graphene, we have carried out diffusion Monte Carlo (DMC) calculations that fully incorporate the electron-electron correlations. Firstly, we obtain Pt-graphene binding energy curves as functions of the vertical distance between Pt and graphene at three different adsorption sites (bridge, on-top, hollow) for both spin states, from which the bridge-site singlet adsorption is found to be the most stable. Furthermore, we reveal a local-minimum feature at the triplet minimum, which results from increasing van der Waals (vdW) interactions with the extended substrate. Our DMC results are compared with DFT results based on several different density functionals, which shows that PBE and rVV10 results are in good agreement with the DMC results for both equilibrium energies and distances. However, the local minimum feature in the triplet region is identified only at the DMC level. Substantial spin-orbit coupling (SOC) effects on the singlet adsorption energy are observed with DFT-PBE calculations while the SOC correction in the triplet state is found to be minimal. With inclusion of the PBE-based SOC correction, the singlet-to-triplet crossing point moves closer to the graphene surface while the local-minimum feature in the triplet region is preserved.

This paper is organized as follows. Computational details of DMC and DFT methods are presented in the section Methodology. DMC results for the adsorption of a single Pt atom on graphene are presented in the section of Results. We summarize our findings and make conclusions in the section Conclusions.

2 Methodology

Our DMC calculations have been performed using the fixed-node method[21] as implemented in the QMCPACK package[22,23]. We used standard Slater-Jastrow type trial wave functions with up to three-body Jastrow factors to describe electron-ion, electron-electron, and electron-electron-ion correlations. The Slater determinants were constructed from plane-wave orbital solutions of spin-polarized DFT Kohn-Sham equations based on the Perdew-Burke-Ernzerhof PBE+U functional[24,25]. As in previous DMC studies for heavy-element materials[26–29], the Hubbard U was treated as a variational parameter in determining the best nodal surface of a trial wave function. We used a plane-wave cutoff of 400 Ry and the $6\times6\times1$ Monkhorst-Pack grids[30] for the PBE+U calculations. All DFT calculations were done using the QUANTUM ESPRESSO package[31].

Norm-conserving scalar-relativistic energy-consistent pseudopotentials by Burkatzki, Filippi and Dolg (BFD)[32,33] were used for C and H atoms. The norm-conserving pseudopotential for a Pt atom was based on 18 semicore and valence electrons with a pseudovalence state of $5s^25p^66s^15d^9$ and its validity was confirmed in a previous DMC study on Pt clusters[34]. The Jastrow parameters were optimized with variational Monte Carlo (VMC) using the linear method of Umrigar *et al.*[35]. Subsequent DMC calculations were carried out with a time step of $\tau = 0.005$ Ha^{-1} and imaginary time projection was done with size-consistent T-moves for variational evaluation of non-local pseudopotentials[22]. To minimize spurious interactions between periodic images, our unit cell of a Pt-graphene complex consisted of a $3\times3\times1$ supercell of graphene and a single Pt adatom (see Fig. 1) and a vacuum distance along the vertical direction was set to 20 Å.

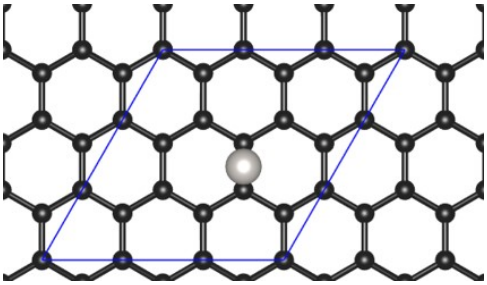

Fig. 1 (Color online) The structure of a single Pt atom adsorbed on the bridge site of graphene. The black- and white-colored spheres represent carbon and Pt atoms, respectively. The blue parallelogram indicates a unit cell consisting of the single Pt atom and the $3\times3\times1$ supercell of graphene.

While the total energy can be exactly estimated from mixed distributions of $\Psi_T(R)\Phi_{FN}(R)$ sampled in an importance-sampled fixed-node DMC process, a mixed estimate of the electron density produces a bias of the order of $\Delta\Psi = (\Psi_T - \Phi_{FN})$ where Ψ_T and Φ_{FN} are the trial and the fixed-node wave functions, respectively. This systematic bias depending on the quality of a trial wave function can be mitigated through an extrapolation between VMC and mixed estimates such as $\rho_{\rm EXT} = 2\rho_{\rm mixed} - \rho_{\rm VMC}$, which is accurate up to the second order of $\Delta\Psi$[21]. The DMC electron densities presented in this study were computed with this extrapolated estimator.

3 Results

In order to study energetics of a Pt atom adsorbed on graphene, we first performed DMC calculations for an isolated Pt atom whose lowest-energy state is a spin triplet. For this, open boundary condition was employed with a $20\times20\times20$ Å^3 cubic simulation box. The atomic energy difference between a spin triplet ground state with electron configuration $6s^15d^9$ and a closed-shell $5d^{10}$ singlet state was estimated in our DMC calculations without SOC to be 0.493(5) eV, which is in excellent agreement with a J-averaged experimental value of 0.478 eV for the ^{3}D-^{1}S splitting of the Pt atom[20,36] (note that the difference between our DMC value and the experimental one is only a third of 1 kcal/mol of the chemical accuracy). On the other hand, the corresponding values estimated with previous quantum chemical calculations based on MP2 and CCSD(T) methods were 0.451[20,36] and 0.486 eV[20], respectively. This confirms the accuracy of our DMC computational setup, including an 18-electron pseudopotential, in dealing with different spin states of a Pt atom adsorbed on graphene. We here considered the ^{1}S$_0$ atomic state, rather than ^{1}D$_2$ that is the lowest-energy spin singlet state of a Pt atom[37], because it is a dominant singlet configuration in a Pt-graphene complex near equilibrium, similar to a Pt atom adsorbed on benzene[20].

We optimized the Hubbard U parameter to obtain the lowest fixed-node energy from trial wave functions made of PBE+U single-particle orbitals. Figure 2(a) shows the fixed-node DMC energy of a Pt-graphene complex as a function of the U value.

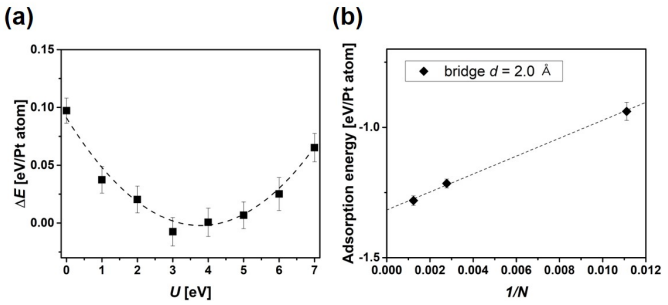

Fig. 2 (a) Fixed-node DMC energy as a function of Hubbard U value in a trial wave function constructed from PBE+U calculations and (b) DMC adsorption energy of a single Pt atom adsorbed at a bridge site of graphene as a function of $1/N$ where N represents the number of electrons in the supercell. While the black dotted line in (a) corresponds to a third-order polynomial fit, the dotted line in (b) represents an extrapolation through a linear fit.

These calculations were done for the $2\times2\times1$ supercell where a single Pt atom was adsorbed at a bridge site and its vertical distance from graphene was set to $d = 2.0$ Å. A third-order polynomial fit of the fixed-node DMC energies resulted in the optimal value of $U = 3.78(8)$ eV, which was used in all DMC calculations presented below. This U optimization procedure was successfully utilized to previous fixed-node DMC studies for heavy-element materials[26–29].

To reduce single-particle finite-size effects, twist boundary conditions[38] were applied in our DMC calculations with 36 twist angles for the $1\times1\times1$ and $2\times2\times1$ supercells and 16 angles for the $3\times3\times1$ supercell. The residual finite-size effects were analyzed through a standard $1/N$ extrapolation. Figure 2(b) displays the adsorption energy of a single Pt atom adsorbed at a bridge site as a function of $1/N$ where N represents the number of electrons in the supercell. The simple-linear regression was used to extrapolate the DMC adsorption energies for the $1\times1\times1$, the $2\times2\times1$, and the $3\times3\times1$ supercells to the thermodynamic limit ($N\rightarrow\infty$). As can be seen in Fig. 2(b), the resulting linear fit was in excellent quality, suggesting that finite-size errors involved in our DMC supercell calculations were resolved adequately.

Based on the aforementioned procedure to produce an accurate fixed-node DMC energy for a given configuration of the Pt-graphene complex, we establish equilibrium binding energetics for a single Pt atom adsorbed at three different sites (bridge, on-top, hollow) at the DMC level. Considering that the ground state of an isolated Pt atom is a spin triplet state, we construct the adsorption energy curves as functions of the Pt-graphene distance, d, separately for spin singlet and triplet states. For spin singlet and triplet states of a Pt-graphene complex, its total magnetic moment is fixed to 0 and 2 μ_B per unit cell, respectively. For this, we used the geometry of the Pt-graphene complex optimized with DFT-PBE calculations for a given d. The Pt adsorption energy is defined by $E_{ad} = E_{\mathrm{Pt-graphene}} - E_{\mathrm{graphene}} - E_{\mathrm{Pt}}$ where E_{Pt} is the energy of an isolated Pt atom in a spin triplet state. Figure 3 presents DMC adsorption energies of a Pt atom adsorbed at each of three adsorption sites for spin singlet and triplet states. Here the solid and the dotted lines represent the Morse potential fits of the corresponding data. Note that the difference between our singlet and triplet adsorption energy curves in the dissociation limit ($d\rightarrow\infty$) corresponds to the DMC singlet-triplet energy difference of 0.493 eV for an isolated Pt atom. As shown in Fig. 3, the Pt adsorptions with the lowest adsorption energies, that is, the equilibrium bindings of a Pt atom to graphene, are found in the singlet curves for all three adsorption sites. The equilibrium adsorption energies are estimated to be -1.33(2), -1.20(3) and -0.65(1) eV/atom for the bridge, the on-top and the hollow site adsorptions, respectively, as tabulated in Table 1. This confirms a conclusion of previous DFT studies based on the generalized gradient approximation (GGA)[8–13] that the bridge site is the most energetically favored adsorption site on graphene for a Pt atom. However, previously-reported GGA adsorption energies at a bridge site are found to be significantly lower than our DMC energy. The magnitude of the equilibrium adsorption energy indicates a covalent bonding between the Pt adatom and C atoms of graphene, accounting for a paired spin configuration at the equilibrium distance. The estimated equilibrium adsorption distances of 1.98(1), 2.00(1), and 1.93(1) Å at bridge, on-top and hollow adsorption sites corresponds to bonding distances of 2.10(1), 2.00(1) and 2.40(1) Å between a single Pt atom and its nearest C atoms. These Pt-C bonding distances at a bridge and an on-top sites are consistent with the sum of the covalent radii of Pt and C atoms[39] while the bonding distance in the hollow-site adsorption is somewhat larger than that. From this, we conclude that chemical bonding at a hollow site have a different nature from those at the other adsorption sites.

As the adsorption distance increases, one can see a crossing point between the singlet and the triplet curves where the favored spin state changes. The single-triplet spin crossing was also predicted in a Pt atom adsorbed on a benzene molecule[20]. According to our DMC calculations, the spin crossings take place at the distances of 2.54 (bridge), 2.58 (on-top), and 2.62 Å (hollow) from a graphene surface, beyond which the second minima determined from the triplet adsorption curves are observed. The equilibrium adsorption energies and distances for spin singlet and triplet states are tabulated Table 1. The energy differences between the triplet minima and the crossing points are estimated to be approximately 0.03, 0.04, and 0.27 eV/atom for bridge, on-top and hollow site adsorptions, respectively. From this, we assign the triplet minima to local minima for the Pt adsorption on graphene. Considering that the adsorption distances ($d > 2.7$ Å) at local minima correspond to Pt-C bonding distances significantly longer that the sum of their covalent radii, we understand that this local minimum feature in the Pt adsorption results from the interplay between weak covalent bonding and vdW interaction. Since the energy barrier at the bridge or on-top site is comparable to thermal energies at room temperatures, the Pt adatom is expected to settle at a local minimum only under low-temperature environment. Note that a Pt atom could diffuse laterally from a hollow site to a bridge or an on-top site with lower adsorption energies.

To obtain a deeper insight into the bonding nature of the Pt-graphene system, we have also investigated Pt-benzene and Pt-coronene systems and compared their binding properties with those of the Pt-graphene system. Figure 4 shows adsorption en-

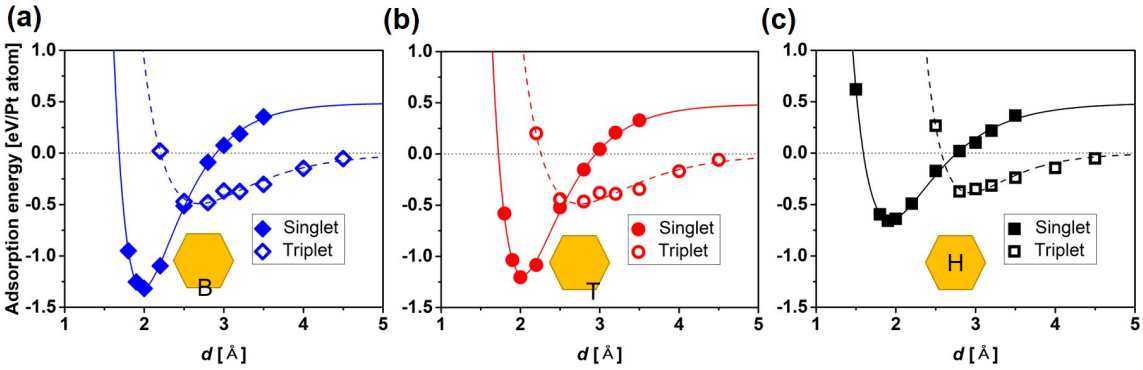

Fig. 3 (Color online) DMC adsorption energy curves of a single Pt atom adsorbed at three different sites of (a) a bridge, (b) an on-top and (c) a hollow site, as a function of the vertical distance from a graphene surface. Here, B, T and H in the insets denote a bridge, an on-top and a hollow adsorption site, respectively. The singlet data are represented by solid symbols while the triplet ones are denoted by open symbols. The solid and the dotted lines represent the Morse potential fits of spin singlet and triplet adsorption energies, respectively.

Adsorption site	E^S	d^S	E^T	d^T
Bridge	-1.33(2)	1.98(1)	-0.49(2)	2.69(3)
On-top	-1.20(3)	2.00(1)	-0.49(3)	2.75(4)
Hollow	-0.65(1)	1.93(1)	-0.38(2)	2.95(3)

Table 1 DMC adsorption energies and vertical distances at the singlet (S) and the triplet (T) minima of a Pt atom adsorbed at three different adsorption sites. The energies and the distances are in units of eV/atom and Å, respectively.

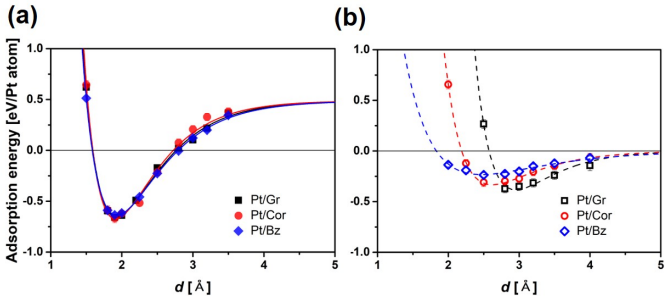

Fig. 4 (Color online) (a) Spin singlet and (b) triplet adsorption energy curve of a single Pt atom adsorbed at a hollow site of graphene (Gr, black), coronene (Cor, red), and benzene (Bz, blue) which were obtained through fixed-node DMC calculations. The axis label d represents the vertical distance from the corresponding substrate. The solid and the dotted lines represent Morse potential fits of the singlet and the triplet data, respectively.

System	E^S	d^S	E^T	d^T
Pt-graphene	-0.65(1)	1.93(1)	-0.38(2)	2.95(3)
Pt-coronene	-0.67(3)	1.91(1)	-0.33(1)	2.62(1)
Pt-benzene	-0.64(1)	1.93(4)	-0.23(1)	2.47(3)

Table 2 DMC adsorption energies and vertical distances at the singlet (S) and the triplet (T) minima of a Pt atom adsorbed at a hollow site of graphene, coronene, and benzene. The energies and the distances are in units of eV/atom and Å, respectively.

ergy curves for a Pt atom adsorbed at a hollow site of graphene, coronene, and benzene. We observe that the singlet curves do not change much depending on the substrate from benezene to graphene. Accordingly, the equilibrium binding properties near the global minima for these three systems are analogous to each other as shown in Table 2 and Fig. 4. This implies that the Pt-graphene interaction at the equilibrium distance from a hollow site mainly stems from the surrounding benzene ring. Thus, the Pt-benzene and the Pt-coronene system can be regarded as reliable fragments to describe the Pt-graphene interaction in the covalent bonding region of the hollow-site adsorption. As the system size increases, on the other hand, the triplet curves are shifted considerably to the right side with a little stronger binding and the singlet-triplet crossing point subsequently moves further away from the substrate. As a result, the local-minimum feature from the triplet state is observed only for a Pt atom adsorbed on the graphene sheet. On molecular substrates of benzene and coronene, the energy barriers from the triplet minimum to the spin-crossing points are not high enough to allow the local minimum feature. Comparison of the triplet curves on different carbon substrates suggests that additive long-range dispersion forces from carbon atoms outside a carbon ring surrounding the Pt adatom are critical in manifesting the local-minimum feature on graphene. We here note that our DMC results for the Pt-benzene system are quantitatively consistent with the corresponding results from previous CCSD(T) and DMC calculations[20], confirming the accuracy of our DMC calculations for the Pt adsorption on carbon substrates.

We now investigate how electrons are redistributed in the ad-

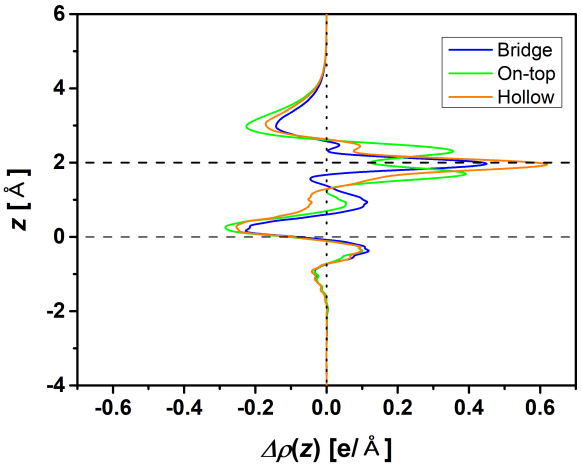

Fig. 5 (Color online) DMC charge density differences between Pt-graphene complexes and the sum of an isolated Pt atom and graphene that are projected onto the vertical z-axis. A Pt adatom in each complex is located at the equilibrium distance from the corresponding adsorption site. A upper (lower) horizontal dashed line represents a z coordinate for a single Pt atom (graphene) while the vertical dotted line represents zero density difference.

sorption process of a Pt atom on graphene. For this, we computed the difference $\Delta\rho$ between the total density of a Pt-graphene complex (ρ^{total}) at an equilibrium geometry and the sum of charge densities of a Pt atom and graphene ($\rho^{Pt} + \rho^{graphene}$), whose projection to the vertical z axis is presented in Fig. 5. A positive sign of $\Delta\rho(z)$ corresponds to charge accumulation at a given location z while charge depletion is represented by its negative sign. One can see in Fig. 5 that charges are drastically redistributed near the Pt adatom (the upper horizontal dashed line) for all three adsorption sites. For the bridge and the on-top sites, one can see charge accumulation in the intermediate region between Pt and graphene, which is compensated by the charge depletion at the upper region of Pt and the lower region of graphene. Unlike the bridge and the on-top site adsorptions, however, charge depletion is observed at the bonding region for the hollow-site adsorption. In conjunction with a higher adsorption energy of -0.66(1) eV/atom at a hollow site, this indicates that a Pt atom adsorbed at a hollow site has different binding nature from the one adsorbed at a bridge or an on-top site. This is also supported by a longer Pt-C bonding distance for the hollow-site adsorption when compared with the bridge or the on-top site adsorption as discussed above.

We now compare our DMC results for the Pt adsorption energy with the corresponding DFT ones based on several different density functionals such as PBE, PBE+D2, rVV10 and vdW-DF2. The DFT adsorption energies of a Pt atom at three adsorption sites, along with the corresponding DMC adsorption curves, are presented in Fig. 6, separately for spin singlet and triplet states. All DFT results agree with our DMC conclusion that the bridge site is energetically the most stable adsorption site. Furthermore, unlike previous DFT studies based on GGA functionals[8–13] where the Pt adsorption energies at equilibrium were lower by $0.1 \sim 0.2$ eV than our DMC results, our DFT-PBE spin-singlet adsorption energy

Table 3 DMC and DFT equilibrium adsorption energy E_s and vertical distance d_s of a Pt atom in a spin singlet state that is adsorbed at a bridge, an on-top, and a hollow site. The energies and the distances are in units of eV/atom and Å, respectively.

Method	Bridge		On-top		Hollow	
	E_s	d_s	E_s	d_s	E_s	d_s
DMC	-1.33(2)	1.98(1)	-1.20(3)	2.00(1)	-0.66(1)	1.89(2)
PBE	-1.31	1.96	-1.13	2.00	-0.64	1.87
PBE+D2	-1.81	1.95	-1.75	2.01	-1.23	1.82
rVV10	-1.35	1.97	-1.23	2.06	-0.68	1.93
vdW-DF2	-0.64	2.11	-0.62	2.16	-0.04	2.23

curves, along with the DFT-rVV10 ones, are consistent with the corresponding DMC curves near the equilibrium distances. This is understood to stem from the fact that our DMC and DFT calculations were based on a semicore+valence 18-electrons pseudopotential for an Pt atom while only valence electrons were considered in previous DFT studies. Consequently, the PBE and rVV10 equilibrium adsorption energies and distances are in good quantitative agreement with the DMC ones as tabulated in Table 3. In addition, charge density redistributions predicted by PBE calculations are also found to be consistent with the corresponding DMC results, both quantitatively and qualitatively, as displayed in Fig. 7 while the rVV10 charge density differences show some discrepancy in the intermediate region from the DMC estimates. Based on this, we conclude that the PBE functional is the most reliable one within the DFT framework in describing the covalent bonding between Pt and graphene near the spin singlet minima. However, PBE fails to predict the long-distance binding of a Pt atom, which can be understood by its well-known limitation in accounting for the vdW interaction. The D2 correction to the PBE results turns out to be about 0.5 eV/atom, significantly larger than an energy scale of typical vdW interaction, and lead to a significant overestimation of the Pt binding energy.

In addition, the triplet minima in PBE, PBE+D2 and rVV10 calculations are located in the region where the singlet state is a favored spin state while the vdW-DF2 results show very broad triplet minima. Consequently, none of the DFT functionals manifests a local-minimum feature in the triplet-favored region. The existence of a local minimum is revealed only in the DMC calculations, implying significance of many-body correlations in describing the Pt binding to graphene at long distances beyond the spin crossing points.

We finally discuss SOC effects on the Pt adsorption on graphene, which were examined only at the PBE level as implemented in the VASP[40]. For the PBE-SOC calculations, the spin is not a good quantum number and is allowed to relax for a given configuration of the Pt-graphene complex. In Fig. 8, the PBE adsorption energy curve at the bridge site with SOC is presented in comparison with the corresponding one without SOC where the lower adsorption energy between the singlet and the triplet energies is presented at each adsorption distance. With inclusion of SOC, the magnetic degrees of freedom is found to be quenched for $d \leq 2.8$, beyond which non-zero magnetic moments emerges. This is consistent with the results from the SOC-free PBE calculations where the spin singlet state is favored at short adsorption

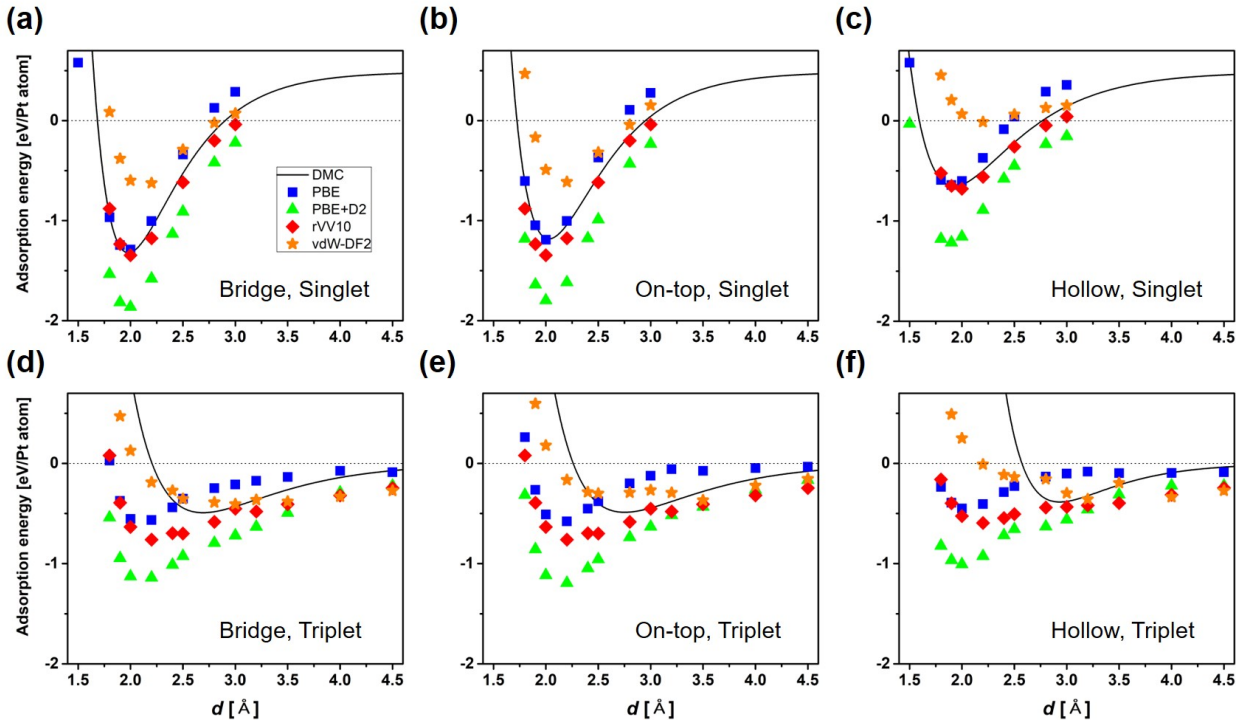

Fig. 6 (Color online) Comparison of DMC adsorption energy of a Pt atom adsorbed at a bridge, an on-top, and a hollow site with the corresponding DFT results computed with several different density functionals. The top panel represents the adsorption energies for spin singlet states and the bottom panel is for spin triplet states. The black solid lines denote the DMC adsorption energy curves and the blue, green, red, and orange symbols represent DFT energies computed with PBE, PBE+D2, rVV10, and vdW-DF2 functionals, respectively.

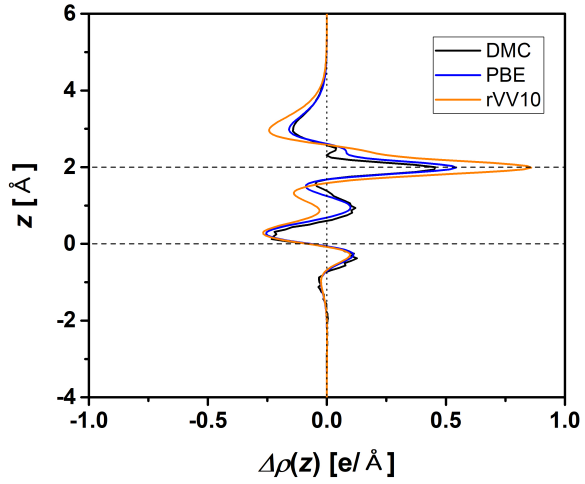

Fig. 7 (Color online) DMC and DFT charge density differences between a Pt-graphene complex and an isolated Pt atom plus graphene that are projected onto the vertical z-axis. A Pt adatom in the complex is adsorbed at a bridge site with a vertical distance of 2.0 Å. A upper (lower) horizontal dashed line represents a z coordinate for a single Pt atom (graphene) while the vertical dotted line represents zero density difference.

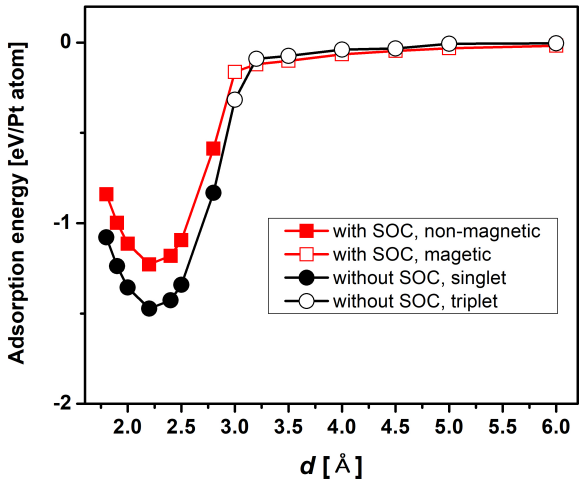

Fig. 8 (Color online) PBE adsorption energy of a Pt atom adsorbed at a bridge site as a function of the vertical distance from a graphene surface with and without SOC. The spin degrees of freedom is allowed to relax in the SOC-incorporated PBE calculations while the lower adsorption energy between the singlet and the triplet energies is presented for the results without SOC. The black solid (open) circles represent the PBE adsorption energies of spin singlet (triplet) states without SOC while the red solid (open) squares represent the PBE-SOC adsorption energies with non-zero (zero) magnetic moments per unit cell.

distances. SOC is seen to substantially weaken the Pt-graphene interaction in the singlet region, reducing the equilibrium binding energy by ~ 0.24 eV/atom, while the SOC effects are found to be minimal, less than 0.03 eV/atom, in the triplet region. Different magnitudes of SOC effects between the singlet and the triplet region were also observed in previous PBE study for the Pt-benzene complex[20]. Larger SOC correction to the singlet adsorption energy is attributed to the fact that the SOC effects are more significant in an isolated Pt atom or in a triplet Pt-graphene complex than in a singlet complex. Considering this, our DMC adsorption curves presented in Fig. 3 are expected to be shifted upward in the singlet region but to change little in the triplet region with incorporation of SOC, which results in the spin crossing point closer to the graphene surface than the one predicted without SOC, along with a higher barrier between the spin-singlet global minimum and the triplet minimum. This leads us to conclude that main qualitative features predicted by our DMC calculations for the adsorption of a single Pt atom on graphene, including the local minimum feature at a long adsorption distance, should be preserved even in the presence of SOC.

4 Conclusions

Fixed-node DMC calculations have been performed for a thorough investigation of the Pt-graphene interaction. We first established the adsorption energy curves of a single Pt atom adsorbed at three different adsorption sites on graphene for both spin singlet and triplet states. The equilibrium Pt adsorptions were observed in the singlet curves, where covalent bondings between a Pt adatom and its neighboring C atoms account for the Pt-graphene interaction. As predicted in previous DFT-GGA studies[8–13], our DMC calculations demonstrate that the most stable Pt adsorption occurs at a bridge site.

According to our DMC calculations, a spin triplet state is favored over a singlet state as a Pt adatom moves further away from a graphene surface. This spin crossing phenomenon was observed to take place at the vertical distances of 2.54 to 2.62 Å from all three adsorption sites on graphene. Furthermore, our DMC calculations reveal a local-minimum feature in the Pt adsorption energy curves, which is understood to be developed as a result of the interplay between weak covalent bonding and vdW interactions in the spin-triplet region. From the fact that none of the DFT functionals considered in this study accounts for this local-minimum feature in the Pt-graphene system, we conclude that many-body correlations incorporated into the DMC calculations are critical for its manifestation. Incorporation of SOC whose effects on the Pt adsoprtion were investigated at the PBE level, would not change main conclusions based on our SOC-free DMC calculations, except that it moves the singlet-triplet crossing points closer to the graphene surface with a higher barrier between a singlet (global) and a triplet (local) minimum.

This work provides a comprehensive picture of the Pt adsorption process on a graphene surface that can be utilized in the development of graphene-based nanoelectronics or Pt catalysis. Finally, our DMC results can serve as a fine starting point to understand the formation of Pt clusters or even Pt layers on graphene, along with the nature of their interaction with graphene, which is currently under our investigation.

Conflicts of interest

There are no conflicts to declare.

Acknowledgements

This paper was supported by Konkuk University in 2019. We also acknowledge the support from the Supercomputing Center/Korea Institute of Science and Technology Information with supercomputing resources (KSC-2019-CRE-0200) that were used for DFT-PBE calculations. H.S and A.B were supported by the U.S. Department of Energy, Office of Science, Basic Energy Sciences, Materials Sciences and Engineering Division, as part of the Computational Materials Sciences Program and Center for Predictive Simulation of Functional Materials. An award of computer time was provided by the Innovative and Novel Computational Impact on Theory and Experiment (INCITE) program and was used to generate all DMC results. This research used resources of the Argonne Leadership Computing Facility, which is a DOE Office of Science User Facility supported under contract DE-AC02-06CH11357.

Notes and references

1 M. Katsnelson, F. Guinea and A. Geim, *Phys. Rev. B*, 2009, **79**, 195426.
2 K. Pi, K. McCreary, W. Bao, W. Han, Y. Chiang, Y. Li, S.-W. Tsai, C. Lau and R. Kawakami, *Phys. Rev. B*, 2009, **80**, 075406.
3 J. Hu, J. Alicea, R. Wu and M. Franz, *Phys. Rev. Lett.*, 2012, **109**, 266801.
4 P. Lazar, J. Granatier, J. Klimeš, P. Hobza and M. Otyepka, *Phys. Chem. Chem. Phys.*, 2014, **16**, 20818–20827.
5 B. Uchoa and A. C. Neto, *Phys. Rev. Lett.*, 2007, **98**, 146801.
6 S. Sun, G. Zhang, N. Gauquelin, N. Chen, J. Zhou, S. Yang, W. Chen, X. Meng, D. Geng, M. N. Banis *et al.*, *Sci. Rep.*, 2013, **3**, 1775.
7 N. Cheng, S. Stambula, D. Wang, M. N. Banis, J. Liu, A. Riese, B. Xiao, R. Li, T.-K. Sham, L.-M. Liu *et al.*, *Nat. Commun.*, 2016, **7**, 13638.
8 K.-j. Kong, Y. Choi, B.-H. Ryu, J.-O. Lee and H. Chang, *Mater. Sci. Eng. C*, 2006, **26**, 1207–1210.
9 K. Okazaki-Maeda, Y. Morikawa, S. Tanaka and M. Kohyama, *Surf. Sci.*, 2010, **604**, 144–154.
10 P. Błoński and J. Hafner, *J. Chem. Phys.*, 2011, **134**, 154705.
11 Y. Tang, Z. Yang and X. Dai, *Phys. Chem. Chem. Phys.*, 2012, **14**, 16566–16572.
12 I. Fampiou and A. Ramasubramaniam, *J. Phys. Chem. C*, 2012, **116**, 6543–6555.
13 X. Liu, Y. Sui, T. Duan, C. Meng and Y. Han, *Phys. Chem. Chem. Phys.*, 2014, **16**, 23584–23593.
14 E. Auer, A. Freund, J. Pietsch and T. Tacke, *Appl. Catal. A: Gen*, 1998, **173**, 259–271.
15 E. Yoo, T. Okata, T. Akita, M. Kohyama, J. Nakamura and I. Honma, *Nano Lett.*, 2009, **9**, 2255–2259.
16 Y. Li, W. Gao, L. Ci, C. Wang and P. M. Ajayan, *Carbon*, 2010, **48**, 1124–1130.

17 H. Wu, D. Wexler and H. Liu, *J. Solid State Electrochem.*, 2011, **15**, 1057–1062.
18 R. Kou, Y. Shao, D. Wang, M. H. Engelhard, J. H. Kwak, J. Wang, V. V. Viswanathan, C. Wang, Y. Lin, Y. Wang *et al.*, *Electrochem. Commun.*, 2009, **11**, 954–957.
19 B. Seger and P. V. Kamat, *J. Phys. Chem. C*, 2009, **113**, 7990–7995.
20 J. Granatier, M. Dubecky, P. Lazar, M. Otyepka and P. Hobza, *J. Chem. Theory Comput.*, 2013, **9**, 1461–1468.
21 W. Foulkes, L. Mitas, R. Needs and G. Rajagopal, *Rev. Mod. Phys.*, 2001, **73**, 33.
22 J. Kim, A. D. Baczewski, T. D. Beaudet, A. Benali, M. C. Bennett, M. A. Berrill, N. S. Blunt, E. J. L. Borda, M. Casula, D. M. Ceperley *et al.*, *J. Phys.: Condens. Matter*, 2018, **30**, 195901.
23 P. R. C. Kent, A. Annaberdiyev, A. Benali, M. C. Bennett, E. J. Landinez Borda, P. Doak, H. Hao, K. D. Jordan, J. T. Krogel, I. Kylänpää *et al.*, *J. Chem. Phys.*, 2020, **152**, 174105.
24 J. P. Perdew, K. Burke and M. Ernzerhof, *Phys. Rev. Lett.*, 1996, **77**, 3865.
25 S. Dudarev, G. Botton, S. Savrasov, C. Humphreys and A. Sutton, *Phys. Rev. B*, 1998, **57**, 1505.
26 Y. Luo, A. Benali, L. Shulenburger, J. T. Krogel, O. Heinonen and P. R. Kent, *New J. Phys.*, 2016, **18**, 113049.
27 A. Benali, L. Shulenburger, J. T. Krogel, X. Zhong, P. R. Kent and O. Heinonen, *Phys. Chem. Chem. Phys.*, 2016, **18**, 18323–18335.
28 K. Foyevtsova, J. T. Krogel, J. Kim, P. Kent, E. Dagotto and F. A. Reboredo, *Phys. Rev. X*, 2014, **4**, 031003.
29 H. Shin, Y. Luo, P. Ganesh, J. Balachandran, J. T. Krogel, P. R. Kent, A. Benali and O. Heinonen, *Phys. Rev. Mat.*, 2017, **1**, 073603.
30 H. J. Monkhorst and J. D. Pack, *Phys. Rev. B*, 1976, **13**, 5188.
31 P. Giannozzi *et al.*, *J. Phys.: Condens. Matter*, 2009, **21**, 395502.
32 M. Burkatzki, C. Filippi and M. Dolg, *J. Chem. Phys.*, 2007, **126**, 234105.
33 M. Burkatzki, C. Filippi and M. Dolg, *J. Chem. Phys.*, 2008, **129**, 164115.
34 W. D. Parker, L. Shulenburger, A. Benali, N. A. Romero and J. Greeley, to be published.
35 C. J. Umrigar, J. Toulouse, C. Filippi, S. Sorella and R. G. Henning, *Phys. Rev. Lett.*, 2007, **98**, 110201.
36 S. Roszak and K. Balasubramanian, *Chem. Phys. Lett.*, 1995, **234**, 101–106.
37 J. E. Sansonetti and W. C. Martin, *J. Phys. Chem. Ref. Data*, 2005, **34**, 1559–2259.
38 C. Lin, F. Zong and D. M. Ceperley, *Phys. Rev. E*, 2001, **64**, 016702.
39 B. Cordero, V. Gómez, A. E. Platero-Prats, M. Revés, J. Echeverría, E. Cremades, F. Barragán and S. Alvarez, *Dalton Trans.*, 2008, 2832–2838.
40 G. Kresse and D. Joubert, *Phys. Rev. B*, 1999, **59**, 1758.